

Characterization of Active Cooling and Flow Distribution in Microvascular Polymers

BRIAN D. KOZOLA,¹ LYLE A. SHIPTON,¹ VINAY K. NATRAJAN,² KENNETH T. CHRISTENSEN² AND SCOTT R. WHITE^{1,*}

¹*Department of Aerospace Engineering, University of Illinois at Urbana-Champaign, Urbana, IL 61801, USA*

²*Department of Mechanical Science and Engineering, University of Illinois at Urbana-Champaign, Urbana, IL 61801, USA*

ABSTRACT: Two- and three-dimensional microvascular networks embedded within a polymer fin were fabricated via direct write assembly to demonstrate cooling potential of vascular polymer structures. Thin fin cooling experiments were carried out utilizing water and poly-alphaolefin (PAO) oil-based coolant as the working fluids. The surface temperature of the fin was monitored using an infrared camera and flow distribution within the network was evaluated by microscopic particle image velocimetry. The effective heat transfer coefficient was increased 53-fold at low Reynolds number for water cooling in both 2D and 3D geometries. However, 3D architectures offer more uniform flow distribution and the ability to efficiently adapt to blockages and reroute flow within the network. Microvascular materials are excellent candidates for compact, efficient cooling platforms for a variety of applications and 3D architectures offer unique performance enhancements.

Key Words: convective heat transfer, polymers, autonomic structures, microfluidics, microvascular networks, infrared imaging, particle image velocimetry.

INTRODUCTION

THERMAL management has become a significant design consideration in modern structural materials and provides an opportunity for multifunctional materials incorporating active cooling. Materials for microelectronics (Tuckerman and Pease, 1981; Wang et al., 2005, Dang et al., 2006; Wei et al., 2007; Oueslati et al., 2008), high power lithium-ion power supplies (Sabbah et al., 2008), fuel cells (Park and Li, 2006; Yu and Jung, 2008), and avionic (Price, 2003) and satellite electronics (Lyll et al., 2008) all require careful thermal management for efficient operation. Reliable thermal control ensures proper function and suitable lifetime in microelectronic systems and prevents malfunctions or catastrophic failure in fuel cells and high output lithium-ion batteries.

Typical cooling systems for power supply and micro-electronic systems have evolved from large scale, conventional heat transfer devices to smaller scale 2D microfluidic devices with channel diameters <1 mm. Microheat exchangers offer an advantage in cooling efficiency due to their small size scale, which maximizes the heat transfer coefficient and increases surface area.

The use of water as a coolant in such systems also provides enhanced performance since it possesses a significantly higher thermal conductivity and heat capacity compared to air. Unfortunately microscale heat transfer devices are complex and expensive to fabricate (via micromachining, stereolithography, chemical etching, and molding (Oueslati et al., 2008)) and difficult to integrate into thermal management systems. As the size of cooling channels is reduced, higher pressures are required to pump the fluid, although parallel architectures and network design can mitigate this effect. Design techniques such as genetic algorithms (Aragon et al., 2008) and constructal design methods (Bejan and Lorente, 2008; Lee et al., 2009) yield optimized networks with lower pressure drops and improved thermal performance.

Microscale fluidic systems have traditionally taken the form of 2D devices with either a single continuous channel or a series of parallel channels. However, network architectures are evolving from these simple 2D devices into complex 3D microvascular materials inspired by biological systems such as capillary blood distribution systems and plant vasculature, which are optimized to efficiently deliver flow to distributed areas. Traditional microfluidic fabrication techniques are largely limited to 2D structures or soft materials that are not well suited for structural applications. In contrast, the direct write assembly technique has been successfully

*Author to whom correspondence should be addressed.
E-mail: swhite@illinois.edu
Figures 2 and 4–12 appear in color online: <http://jim.sagepub.com>

used to create complex 3D networks embedded within structural polymers and it shows great promise for complex, biomimetic microvascular networks.

Direct write assembly is an efficient fabrication method, which enables printing of 3D template structures using a fugitive organic ink (Therriault et al., 2003; Lewis, 2006). Subsequent infiltration of the template with a polymer matrix and removal of the sacrificial template yields a microvascular polymer with 3D interconnectivity. Channel sizes ranging from 1 μm to over 1 mm are possible (Lewis, 2006) and networks can be stacked and interconnected vertically to create complex 3D networks (Therriault et al., 2003, 2005; Lewis, 2006). While other fabrication techniques may also produce layered 3D networks, direct write assembly offers a facile process with more inherent design flexibility and lower cost. Direct write assembly has been used previously to fabricate highly efficient 3D micromixers (Therriault et al., 2003), multifunctional self-healing materials (Toohey et al., 2007; Hansen et al., 2009), and a 2D self-cooling printed circuit board (Oueslati et al., 2008).

In this study we use the direct write assembly technique to create 2D and 3D microvascular networks for active cooling of a heated polymer fin. Three network architectures are examined to investigate the effect of channel size and dimensionality. Both water and a commercial polyalphaolefin (PAO) oil-based coolant

(Paschkewitz, 1998; Sleiti, 2007) are used as working fluids with flow rates ranging from 1 to 10 mL/min. The transient and steady-state thermal responses were investigated using an infrared (IR) camera and the flow through individual channels was measured using microscopic particle image velocimetry ($\mu\text{-PIV}$) measurements.

MATERIALS AND METHODS

The microvascular materials examined in this study consist of 2D and 3D vascular networks embedded within an epoxy matrix. The epoxy matrix used is Epon 828 (Hexion Specialty Chemicals) resin and Epicure 3274 (Hexion Specialty Chemicals) amine curing agent at a ratio of 2.5:1 by mass.

Specimen Design

A thin fin geometry (Figure 1) was used for all testing. The thin fin configuration provided a convenient and well-characterized 2D temperature field for experimental testing and analysis. A microvascular network was embedded in the center of the specimen, 18.4 mm long \times 18.4 mm tall, and centered along the length of the fin. The vascular network was connected to inlet and outlet ports via fanning manifolds of the same

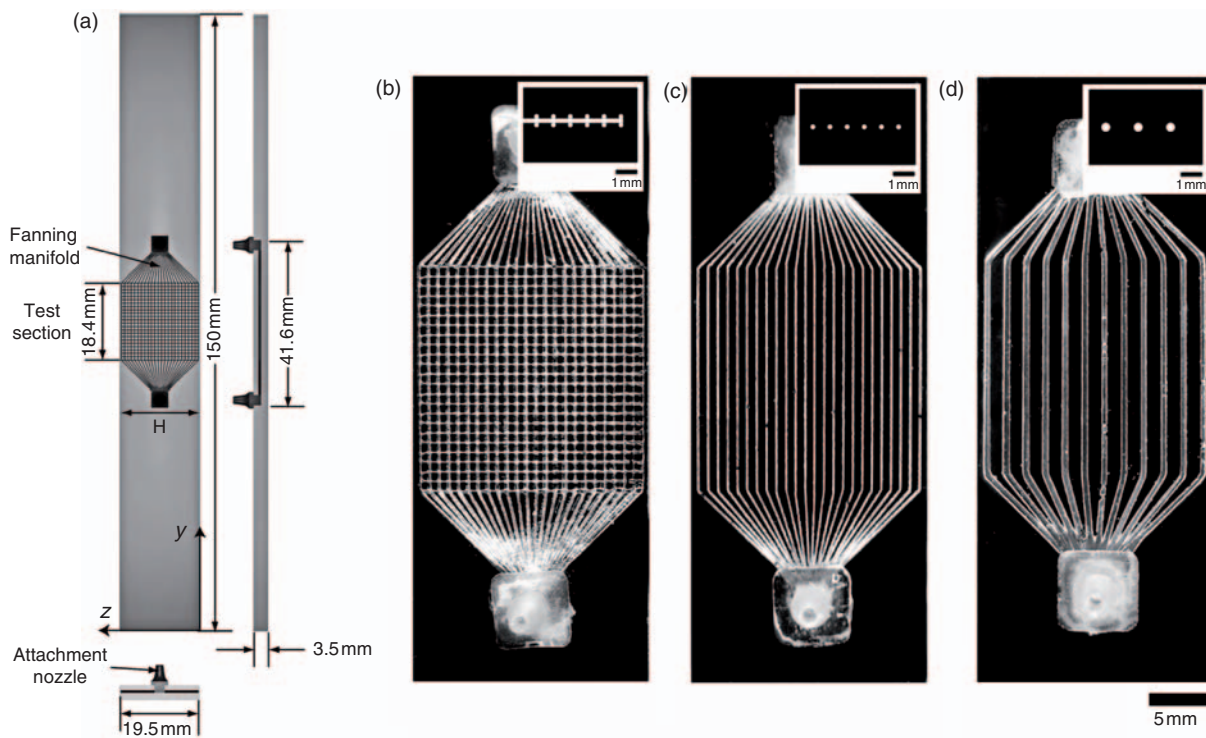


Figure 1. Microvascular fin and network geometry. (a) Details of fin specimen with embedded three-layer microvascular network. (b–d) Images of specimens tested with insets of specimen cross sections: (b) 3D network (200 μm diameter), (c) 24-channel array (200 μm diameter), (d) 12-channel array (410 μm diameter).

diameter as the network channels, and each manifold spans 9.2 mm from the edge of the network to the inlet and outlet junctions. These junctions connect directly to the barbed nozzles and measure 2.4 mm square \times 1.8 mm tall. The three-layer specimen contains three-layer manifolds that feed directly into and out of each layer such that they feed directly into the parallel channels in the top and bottom layers and into the edge of the first channel in the middle, perpendicular, layer.

Four types of samples were prepared. First, a solid epoxy fin was fabricated as a control to verify the thin fin approximation and determine if the presence of an air-filled microvascular network affected the temperature profile of the fin. Two types of 2D network specimens with roughly equal channel surface areas were fabricated consisting of a series of parallel microchannels spanning 18.4 mm along the length. The first 2D specimen, shown in Figure 1(c), contains 24 parallel channels of 200 μ m diameter, which are spaced 800 μ m from center to center. The second type of 2D specimen, shown in Figure 1(d), consists of 12 parallel microchannels of 410 μ m diameter spaced 1600 μ m from center to center. One 3D network specimen was also fabricated consisting of three layers of 24 parallel 200 μ m diameter channels spaced 800 μ m from center to center and vertically interconnected. The top and bottom layers are aligned parallel to the fin length (y -direction) while the center layer is oriented perpendicular (z -direction). The multilayer geometry is shown in Figure 1(b) and the layers are interconnected vertically at every cross-over point formed where the channels in one layer touch the array of channels in the underlying layer.

Specimen Fabrication

Fabrication of samples was accomplished through a combination of direct-write assembly (Lewis, 2006) and molding. In the first stage a substrate was fabricated by partially filling a silicone rubber mold with the epoxy matrix and then allowing the epoxy to gel for 18 h at room temperature ($\sim 23^\circ\text{C}$). Subsequently, a fugitive organic ink template of the microvascular network was written onto the substrate surface at a rate of 10 mm/s using a robotically controlled deposition device (Aerotech Inc.), Figure 2(a). Total deposition time

ranged from 75 s for the 12-channel array to 341 s for the 3D network. The fugitive organic ink (Hansen et al., 2005) consists of a mixture of microcrystalline wax (SP-19, Strahl and Pitsch) and heavy mineral oil (Fisher Scientific) and is extruded onto the substrate at constant pressure (350 psi) through a cylindrical micro-nozzle with a diameter equal to the desired channel diameter (200 or 410 μ m).

After the ink has been deposited, a mating silicone rubber mold is placed on top and the mold is infiltrated with epoxy (Figure 2(b)). The epoxy matrix is then cured at room temperature ($\sim 23^\circ\text{C}$) for 24 h followed by an additional 2 h at 50°C (Figure 2(c)). After curing, the fugitive ink is removed by heating the sample (75°C) to melt the ink and applying light vacuum to evacuate the wax (Figure 2(d)). A final cleansing of the network is performed by passing hot water, hexane, and deionized water consecutively through the microchannels to remove any remaining ink.

The specimens were cut and sanded to the desired final dimensions and one side was polished to improve optical clarity for imaging experiments while the other side was painted matte black (Krylon, Ultra-Flat Black) for imaging with an infrared camera. Barbed polypropylene nozzles were attached to the inlet and outlet port of each sample using cyanoacrylate for connection to a precision syringe pump and an output reservoir.

Flow Testing

The flow in individual channels of each specimen was characterized using the μ -PIV technique to acquire ensembles of instantaneous velocity realizations in a plane spanning the full diameter of the individual microchannels at depth center. This technique allows the instantaneous fluid velocity field on a specific plane within the flow to be inferred via analysis of pairs of time-delayed images of inertial tracer particles present within the fluid (Santiago et al., 1998). Figure 3 shows a schematic of the experimental setup employed. A solution of deionized water seeded with 2 μ m polystyrene microspheres containing fluorescent Nile red dye (Invitrogen, Fluospheres[®]) with a peak emission wavelength at $\lambda = 575 \mu\text{m}$ was pumped through the microvascular networks at a constant flow rate using a syringe

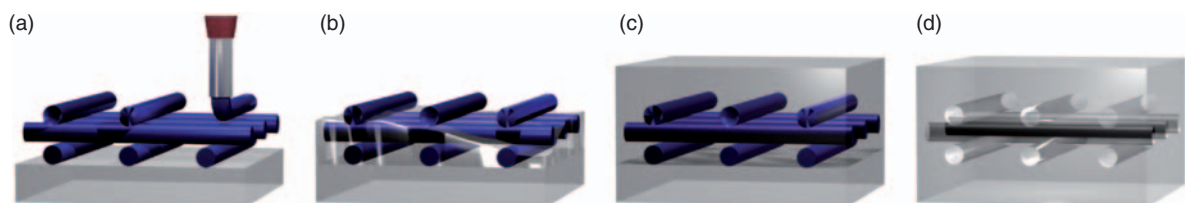


Figure 2. Schematic representation of the direct write fabrication procedure: (a) ink deposition on cured substrate, (b) epoxy infiltration of completed network, (c) cured specimen, (d) specimen after evacuation of fugitive ink.

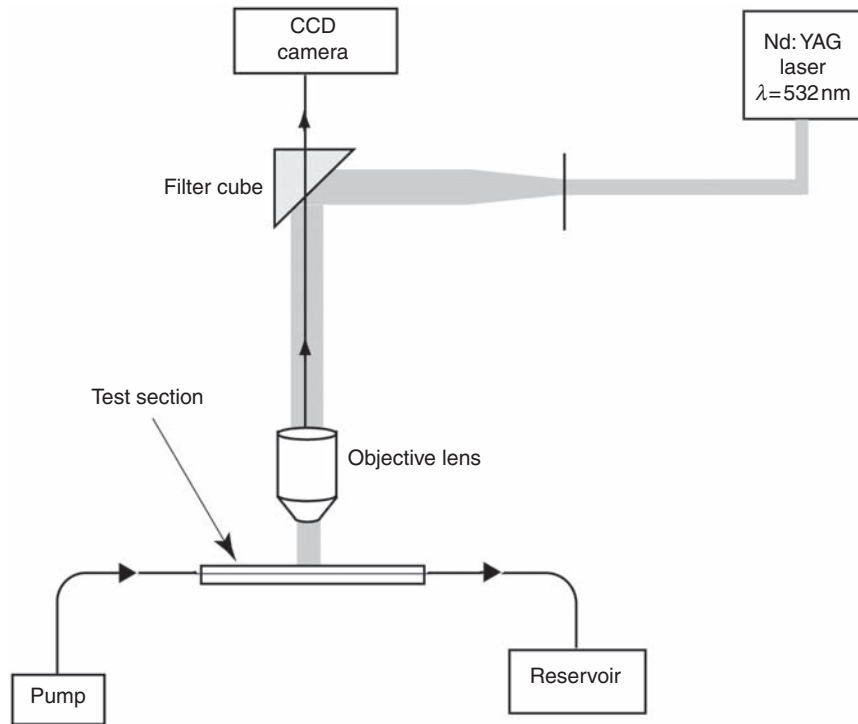


Figure 3. μ -PIV experimental setup.

pump (Harvard Apparatus, PHD2000). All measurements were conducted at times beyond the transient start-up of the system. The field of view was volume-illuminated with a double-pulsed Nd:YAG laser ($\lambda = 532$ nm, Continuum). Each beam was directed through an epi-fluorescent filter cube via an entry port located at the rear of the microscope (Olympus BX60) followed by passage through a $10\times$ (N.A. = 0.30) microscope objective lens that guided the light to the specimen. The emission from the particles passed through the filter cube while the incident wavelength was blocked, ensuring only the fluoresced light from the particles was imaged by the $2k \times 2k$ pixel, 12-bit frame-straddle CCD camera (TSI, 4MP). The seeding density of the tracer particles was optimized to a volume fraction of 0.020% in deionized water. For each flow rate examined, the time delay between two successive images in a pair was adjusted to yield bulk particle displacements of roughly 8 pixels. The μ -PIV images were interrogated using two-frame cross correlation methods which yielded vector grid spacings of $\Delta x = \Delta y = 11.91 \mu\text{m}$ in the axial and transverse directions, respectively. The instantaneous vector fields were then validated using standard deviation and local magnitude difference comparisons to remove erroneous velocity vectors (Christensen et al., 2000). The few holes (<3%) generated by this validation process were filled either with alternative velocity choices determined during the interrogation or interpolated in regions where at least 50% of neighbors were present. Each instantaneous vector field

was then low-pass filtered with a narrow Gaussian filter to remove any noise associated with frequencies larger than the sampling frequency of the interrogation.

Thermal Testing

Thermal measurements were accomplished by infrared imaging of the specimen front surface (Figure 4). The bottom edge of the sample was placed on a copper plate held at constant temperature (80°C) and a thin layer of OmegaTherm[©] thermally conductive grease was used along the interface between the fin and plate. The copper plate was heated using a Watlow[©] 120 V, 200 W resistive heater attached to the bottom of the plate and controlled with a Watlow[©] Series 942 microprocessor to maintain a top surface temperature of $80 \pm 1^\circ\text{C}$. The feedback control thermocouple was permanently bonded to the top surface of the plate and an additional thermocouple was placed in the thermal grease between the fin and the plate at the center of the specimen to verify constant temperature boundary condition throughout testing. The entire sample and plate was enclosed within a Plexiglas box to prevent losses from convective currents in the laboratory environment.

Infrared images were taken using a DeltaThermTM 1560 infrared camera with a 320×256 array of Indium Antimonide infrared detectors yielding a spatial resolution of $110 \mu\text{m}$ within the field of view. Data was recorded at one frame per second for transient cooling

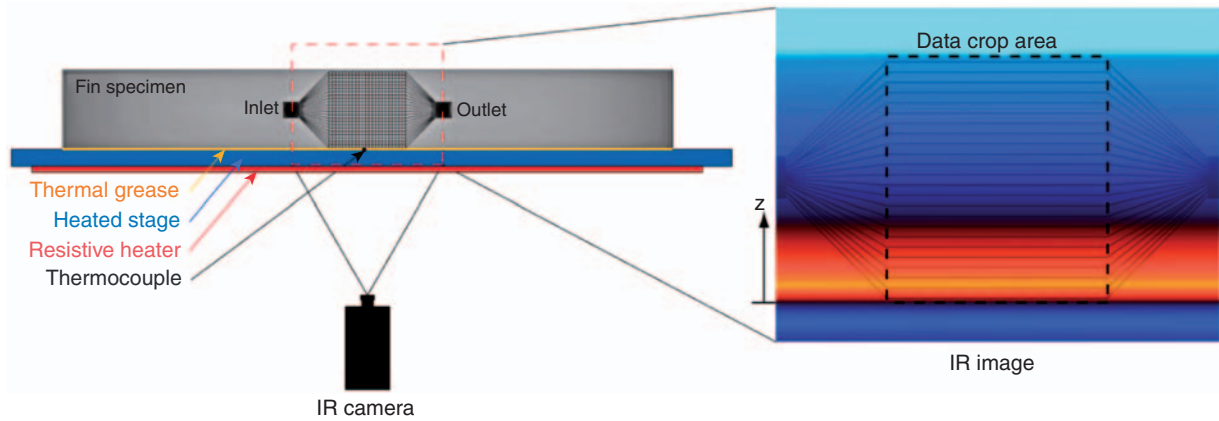


Figure 4. Thermal imaging experimental setup (left) and infrared thermal image of specimen (right).

tests, and 20 s of data was averaged every 5 min over a duration of 1 h for steady-state experiments.

Infrared image data was collected via DeltaVision™ software running on a Windows XP based computer. The data was subsequently analyzed frame by frame in MatLAB™ (R2009a) to convert pixel intensity value to temperature and crop the data field to the 18.4 mm × 19.5 mm area of interest over the cooling network. Each data set results in a unique 2D temperature field of the specimen surface. In order to compare the system cooling performance across sample types and conditions, the mean field temperature was calculated by averaging all pixels within the cropped field of view.

Two different working fluids were used in these experiments. The bulk of testing was carried out with deionized water as the coolant at various flow rates from 1 to 10 mL/min. In addition, a military certified (MIL-PRF-87252) coolant based on a polyalphaolefin (PAO) oil was also examined. PAO oil coolants possess lubricating and anticorrosive properties and have been used in aerospace applications such as cooling avionics and electric rotors (Paschkewitz, 1998; Price, 2003; Sleiti, 2007). The fluids were introduced to the sample at 20°C at a constant flow rate through the use of a screw driven syringe pump (KD Scientific, Model 210).

RESULTS

A series of experiments was carried out on microvascular cooling of thin epoxy fins at a variety of flow rates, network geometries, and working fluids. Thin fin validation experiments were also carried out for the experimental conditions employed.

Thin Fin Validation

A validation test was performed on a solid epoxy fin to compare the steady-state thermal profile to the analytical solution for a 2D thin fin. The thin fin

approximation assumes that temperature is uniform through the thickness of the fin, meaning that heat flow is 1D along the height (z -direction). The governing equation for heat transfer in this case is:

$$\frac{d^2 T}{dz^2} - \frac{hP}{kA_c}(T - T_\infty) = 0, \quad (1)$$

where T is the temperature, h is the heat transfer coefficient for the interface between the solid and fluid, P is the total length of the perimeter of the sample, k is the thermal conductivity of the fin material, A_c is the cross-sectional area of the fin, and T_∞ is the temperature of the environment surrounding the fin. Solving this governing ordinary differential equation for a constant temperature boundary condition of $T(z = 0) = T_b$ yields the solution:

$$\frac{T - T_\infty}{T_b - T_\infty} = \frac{\cosh \beta(H - z) + \left(\frac{h}{\beta k}\right) \sinh \beta(H - z)}{\cosh \beta H + \left(\frac{h}{\beta k}\right) \sinh \beta H}, \quad (2)$$

where T_b is the temperature of the heated stage, H is the fin height, and $\beta = \sqrt{hP/kA_c}$.

The thermal conductivity (k) of the epoxy was measured using a modified Lee's Disk method, which has been shown to correlate well with national test standards (Price and Jarratt, 2002). The test set up utilized the Watlow© resistive heater (previously described) to heat an aluminum plate, while a thin specimen of epoxy (3.01 mm thick and 57.5 mm in diameter) was sandwiched between the heated plate and another identical aluminum plate. The temperatures of the plates were measured using J-type thermocouples as 64°C and 54°C, respectively, upon reaching equilibrium. Subsequently, the convective heat loss (h) of the unheated plate was measured to be 1.96 W/m²K and

the thermal conductivity (k) for this temperature range was calculated with Equation (3):

$$k = \frac{ht}{A(T_1 - T_2)}, \quad (3)$$

where A , t , T_1 , and T_2 are the sample cross-sectional area and thickness, and the temperatures of the heated and unheated aluminum plates, respectively. Using the temperature values at equilibrium and specimen dimensions, the thermal conductivity of Epon 828/Epicure 3274 epoxy was calculated to be 0.228 W/m K in the 54–64°C temperature range.

A plot of the thermal profile along the fin length for a solid epoxy fin at steady state is shown in Figure 5. Overlaid on this plot is the analytical thin fin solution where a least squares fit of the heat transfer coefficient yields $h = 3.70 \text{ W/m}^2 \text{ K}$. The two profiles differ at most

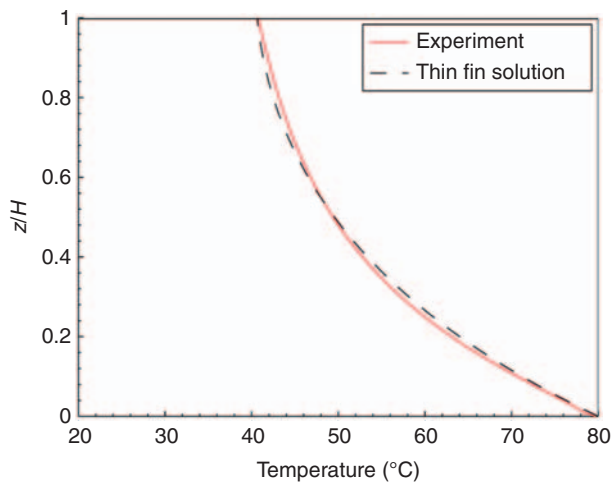


Figure 5. Vertical temperature profile for solid epoxy fin specimen at steady state.

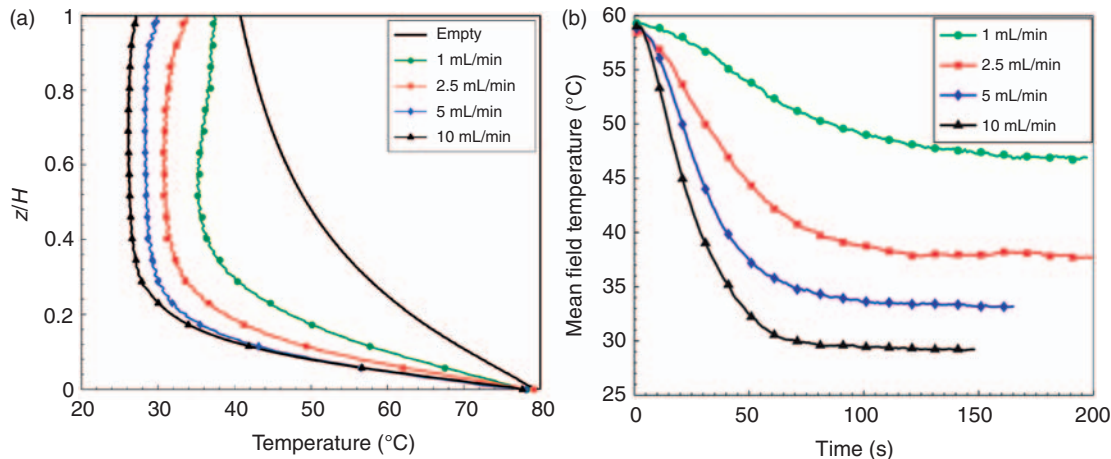


Figure 6. Effect of flow rate on thermal profiles for water cooling through 24-channel array (200 μm diameter) network: (a) steady-state temperature profile, (b) transient response of mean field temperature.

by 1.03°C (at $z/H=0.24$) and have an RMS error of 0.60°C.

Effect of Flow Rate

The effect of flow rate on cooling performance was analyzed for the 24-channel array (200 μm diameter) network (Figure 1(b)) by circulating water (20°C inlet temperature) at 1, 2.5, 5, and 10 mL/min. Figure 6 shows the steady-state temperature profiles and transient responses after commencing circulation. The thermal characteristics of a sample with empty channels are included for comparison. Increased flow rate results in lower steady-state temperatures and faster cooling rates. The maximum decrease in temperature was 35°C at approximately 20% of the fin height at 10 mL/min compared to the empty-channel case. However, even the lowest flow rate of 1 mL/min provides significant cooling with a reduction in the mean field temperature of 15°C at steady-state conditions.

The steady-state temperature profiles were modeled with Equation (2) to determine an effective heat transfer coefficient (h_{eff}) due to the embedded microvascular system. The thermal conductivity and all other parameters were maintained constant while adjusting the heat transfer coefficient to fit the temperature profiles in Figure 6(a). The results are presented in Table 1 along with the least squares quality of fit (R^2). Active cooling

Table 1. Effective heat transfer coefficient for 24-channel single-layer specimen with water cooling.

Q (mL/min)	k (W/m K)	h_{eff} (W/m ² K)	R^2
0	0.228	3.70	0.997
1	0.228	15.6	0.808
2.5	0.228	51.8	0.928
5	0.228	111	0.989
10	0.228	198	0.908

effectively increases the heat transfer coefficient 53-fold for 10 mL/min water circulation compared to the fin with empty channels.

Flow analysis using μ -PIV experiments reveal the distribution of flow within the microvascular network and how it changes with flow rate. The Reynolds number ($\equiv UD/\nu$, where U is the characteristic velocity, D is the channel diameter, and ν is the kinematic viscosity of the working fluid) for 200 μm diameter microchannels ranges from 12 to 122 for the flow rates tested, which is well within the laminar flow regime. Flow distribution for each microchannel at low and high flow rates are shown in Figure 7 where the channels are numbered from 1 at the bottom of the specimen ($z/H=0.03$) to 24 at the top of the specimen ($z/H=0.97$). While all channels exhibit active flow at both flow rates, there is notably higher variability in the flow at lower flow rates. At higher flow rates this effect diminishes and a more uniform flow is achieved. Slightly lower flow rates are apparent at the top and bottom of the sample as a consequence of longer flow path (7.6 mm) due to the fanning manifold design (Figure 1) and sharper angle transitions into the channel network. Assuming Poiseuille flow, the increased channel length causes an 11% decrease in flow rate in the edge channels. The standard deviations in flow rate across the network as a function of input flow rate are shown in Table 2.

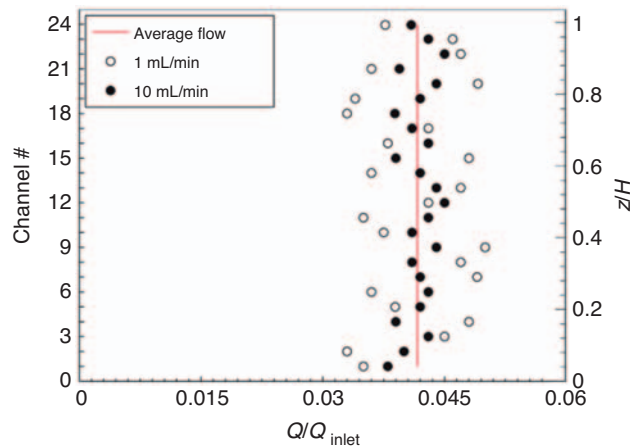


Figure 7. Flow mapping of individual channels in the 24-channel array (200 μm diameter) network.

Table 2. Standard deviation of Q/Q_{inlet} in individual channels.

Flow rate (mL/min)	Standard deviation ($\times 10^{-3}$)		
	24-channel network	12-channel network	3-layer network
1	5.98	21.6	—
5	3.90	10.4	0.692
10	2.01	4.35	—

Effect of Network Geometry

The transient cooling results for all three network geometries at a flow rate of 5 mL/min are shown in Figure 8. The most prominent effect on cooling performance is that of channel size. While the single layer 200 and 410 μm network samples have roughly the same channel surface area, the 200 μm network cools 73% faster and reduces the mean field temperature an additional 33% compared to the 410 μm network. Increased performance with smaller diameter channels is due to increased heat transfer coefficient and finer distribution of channels, and highlights the significant advantages of leveraging small size scales for microvascular cooling.

The flow analysis for the 410 μm network is shown in Figure 9 and Table 2. Again, flow fluctuations across the channels are pronounced at low rates and are smoothed

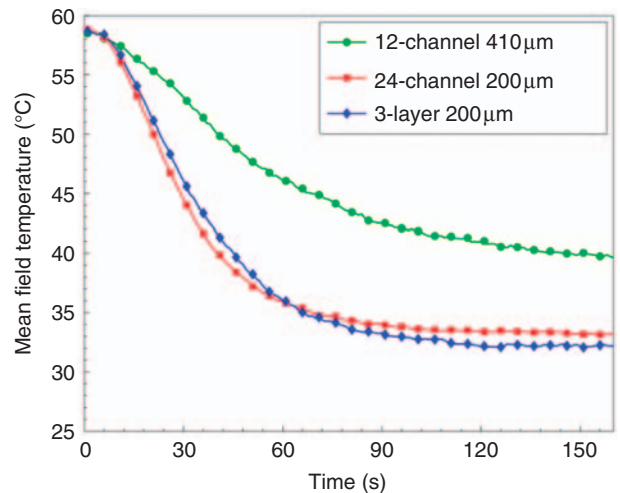


Figure 8. Transient cooling results for all network geometries at 5 mL/min water.

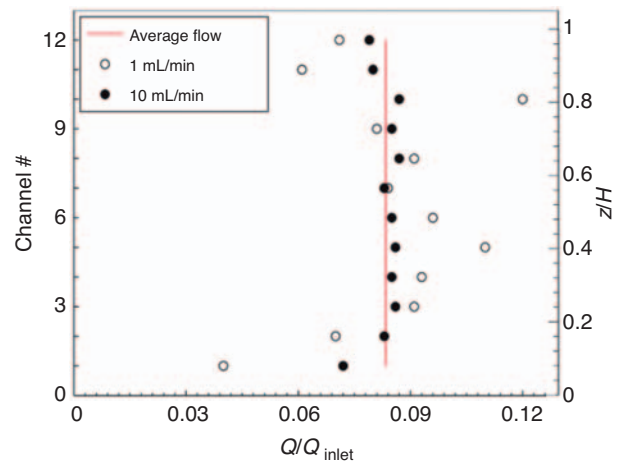


Figure 9. Flow mapping of individual channels in the 12-channel array (410 μm diameter) network.

as the inlet flow rate is increased. Compared to the single layer 200 μm network, these fluctuations are much more pronounced.

Comparing single and three layer networks at 200 μm channel diameter, very similar cooling performance is obtained even with the three-fold increased heat transfer area provided by the three-layer network. While the single-layer network has a slightly faster initial cooling, equilibrium is reached at similar times and the three-layer specimen shows a 4% lower final mean field temperature. Potential disadvantages of the 3D network

include increased channel volume and liquid coolant present in the polymer structure, and increased susceptibility to leakage due to damage or defects. However, the primary advantage of 3D networks is revealed by the μ-PIV data. Three dimensionality provides additional interconnectivity of the flow paths, which yields a much more uniform flow distribution compared to the single-layer systems as shown in Figure 10.

Flow analysis for the three-layer specimen was particularly challenging given the need to illuminate and image subsurface features within the vascular network. Only the top and middle layers were successfully analyzed since the bottom layer was directly registered and optically obscured by the top layer. Figure 11 shows the fluid flow distribution in the top and middle layers for flow passing from left to right. Fully 92% of the flow is approximately evenly distributed between the top and bottom layers, which have channels parallel to the flow direction, and only 8% of the flow occurs in transversely oriented middle layer.

Although the middle layer only carries 8% of the total flow, it does aid significantly in redistributing the flow throughout the network which results in highly uniform flow distribution in the bottom and top layer channels. The leftmost channels (those closest to the inlet) carry flow in the vertical direction to equalize the distribution in the top and bottom layers. As the fluid moves across the specimen (left to right), the distribution of flow in the top/bottom layer is nearly uniform and flow in the middle layer diminishes to a negligible amount. Importantly, any obstruction in the network can be

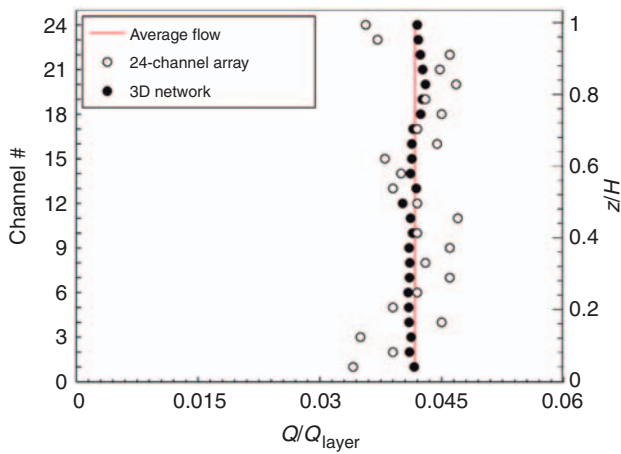


Figure 10. Flow in 24-channel array (200 μm diameter) and 3D network at 5 mL/min. Q_{layer} corresponds to total volumetric flow measured in the layer evaluated.

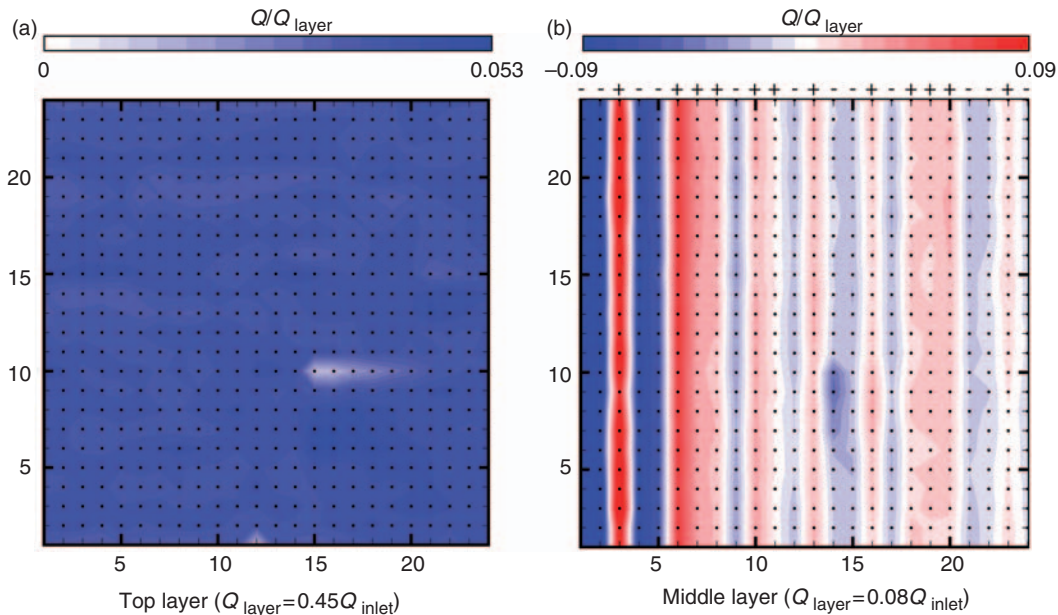


Figure 11. Flow mapping for 3D network (200 μm diameter): (a) results for top layer with flow traveling from left to right, and (b) results for middle layer with channels oriented perpendicular to the flow direction. Blue indicates flow traveling from bottom to top of network and red indicates downward flow.

circumvented by rerouting flow through the middle layer. For example, Figure 11(a) shows an obstruction (likely a manufacturing defect) located in the grid network at position (15,10) where the flow in the top layer is completely blocked. The 3D interconnected design of the three-layer network allows for flow to be efficiently redirected into the middle layer and then back into the top layer so that uniform flow is reestablished only 4 mm downstream of the obstruction.

Effect of Working Fluid

In addition to water a PAO oil-based fluid was also tested to evaluate system performance using a military certified (MIL-PRF-87252 Performance Standard) coolant. The PAO oil was tested in the single-layer 200 μm network and the transient cooling results are presented in Figure 12 in comparison to water. While cooling performance is very similar, water shows a faster cooling rate with a lower steady-state temperature for every flow rate tested. In comparison to PAO oil, water has a higher specific heat (4.18 vs. 2.21 J/g K) and higher thermal conductivity (0.58 vs. 0.14 W/m K), leading to enhanced cooling performance. In addition, PAO oil is notably more viscous than water with a viscosity ranging from 1.65 to 5 times that of water at 100°C and 40°C, respectively (MIL-PRF-87252 Performance Standard, Kleemola and Lehtovaara, 2008).

However, PAO oil was found to wet the microvascular network much better than water so that entrapment of air was less of a problem. Most importantly, PAO oil coolant is non-corrosive, lubricating, and has a much wider operating temperature range of -54°C to 200°C .

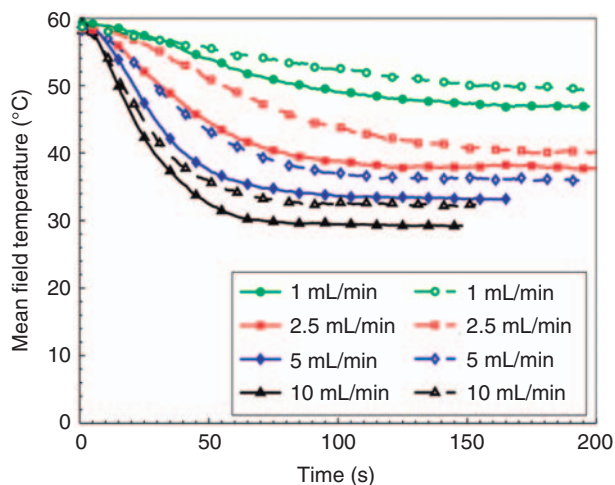


Figure 12. Transient cooling results for water (solid symbols) and PAO oil (open symbols) over a range of flow rates (1–10 mL/min) in 24-channel array network.

CONCLUSIONS

We have clearly demonstrated that embedded 2D and 3D microvascular networks in polymers can efficiently cool these materials at low Reynolds number. The effective heat transfer coefficient in a thin fin geometry was increased by 53-fold at 10 mL/min water flow rate. Cooling performance depends on the thermal and physical properties of the working fluid, flow rate, and network architecture. Water was a better coolant over the temperature range and flow rates studied compared to PAO oil. While fast cooling and lower steady-state temperatures were achieved at the highest flow rate studied (10 mL/min), increasing the flow rate further will eventually show a plateau in performance as the fluid outlet temperature approaches that of the inlet, and the channels act as constant temperature heat sinks.

Decreasing the channel diameter from 410 to 200 μm increased the magnitude and rate of cooling, even when the channel wall surface area was held roughly constant. These results highlight one of the primary advantages of microvascular cooling in which the small size scale yields higher heat transfer coefficients, a finer distribution of the coolant within the volume, and better cooling efficiency at a given volumetric flow rate.

Three-dimensional, multilayer networks provide two advantages compared to single layer networks. First, the 3D flow paths provide a mechanism for smoothing of the flow and results in more uniform distribution throughout the network. Secondly, interconnectivity of flow paths in 3D networks provides flow path redundancy so that defects in the network can be quickly circumvented and system performance maintained.

ACKNOWLEDGMENTS

The authors would like to thank Dr Andrey Voevodin and Dr Lois Gschwender of the AFRL Thermal Sciences and Materials Branch for providing the MIL-PRF-87252 coolant for testing in this study.

FUNDING

This work was supported by the Air Force Office of Scientific Research [MURI Grant No. F49550-05-1-0346].

REFERENCES

- Aragon, A.M., Wayer, J.K., Geubelle, P.H., Goldberg, D.E. and White, S.R. 2008. "Design of Microvascular Flow Networks Using Multi-objective Genetic Algorithms," *Computer Methods in Applied Mechanics Engineering*, 197:4399–4410.

- Bejan, A. and Lorente, S. 2008. *Design with Constructal Theory*, Wiley, Hoboken, NJ.
- Christensen, K.T., Soloff, S.M. and Adrian, R.J. 2000. "PIV Sleuth: Integrated Particle Image Velocimetry Interrogation/Validation Software," TAM Report 943, University of Illinois at Urbana-Champaign.
- Dang, B.M., Bakir, M.S. and Meindl, J.D. 2006. "Integrated Thermal-Fluidic I/O Interconnects for an On-chip Microchannel Heat Sink," *IEEE Electron Device Letters*, 27:117–119.
- Hansen, C.J., Wu, W., Toohey, K.S., Sottos, N.R., White, S.R. and Lewis, J.A. 2009. "Self-healing materials with interpenetrating microvascular networks," *Advanced Materials*, 21:4143–4147.
- Kleemola, J. and Lehtovaara, A. 2008. "An Approach for Determination of Lubricant Properties at Elliptical Elastohydrodynamic Contacts Using a Twin-disc Test Device and a Numerical Traction Model," *Proceedings of the Institution of Mechanical Engineers, Part J: Journal of Engineering Tribology*, 222:797–806.
- Lee, J., Lorente, S., Bejan, A. and Kim, M. 2009. "Vascular Structures with Flow Uniformity and Small Resistance," *International Journal of Heat Mass Transfer*, 52:1761–1768.
- Lewis, J.A. 2006. "Direct Ink Writing of 3D Functional Materials," *Advanced Functional Materials*, 16:2193–2204.
- Lyll, M.E., Williams, A.D., Arrit, B.J. and Taft, B.S. 2008. "Experimental Analysis of a Biologically Inspired Thermal-Structural Satellite Panel," In: *49th AIAA/ASME/ASCE/AHS/ASC Structures, Structural Dynamics, and Materials Conference*, 7–10 April, American Institute of Aeronautics and Astronautics Inc., Reston, VA 20191, USA.
- Oueslati, R.B., Therriault, D. and Martel, S. 2008. "PCB-integrated Heat Exchanger for Cooling Electronics Using Microchannels Fabricated with the Direct-write Method," *IEEE Transactions on Components and Packaging Technologies*, 31:869–874.
- Park, J. and Li, X. 2006. "Effect of Flow and Temperature Distribution on the Performance of a PEM Fuel Cell Stack," *Journal of Power Sources*, 162:444–459.
- Paschkewitz, J.S. 1998. "Exposure Testing of Dielectric Liquids for Aircraft EHD Heat Exchanger Applications," In: *IEEE: Conference on Electrical Insulation and Dielectric Phenomena (CEIDP)*, 25–28 October, Atlanta, GA, Annual Report 1, pp. 166–169.
- Price, D.C. 2003. *Thermal Management of Military Fighter Aircraft Electro-optics Pod: An Invited Paper*, Institute of Electrical and Electronics Engineers Inc, New York, NY.
- Price, D. and Jarratt, M. 2002. "Thermal Conductivity of PTFE and PTFE Composites," *Thermochimica Acta*, 392–393:231–236.
- Sabbah, R., Kizilel, R., Selman, J.R. and Al-Hallaj, S. 2008. "Active vs. Passive Thermal Management of High Power Lithium-ion Packs," *Journal of Power Sources*, 182:630–638.
- Santiago, J.G., Wereley, S.T., Meinhart, C.D., Beebe, D.J. and Adrian, R.J. 1998. "A Particle-image Velocimetry System for Microfluidics," *Experiments in Fluids*, 25:316–319.
- Sleiti, A.K. 2007. "Advanced Cooling Technology for Rotors of High-power Low-duty Cycle Generators Using Polyalphaolefins," *Journal of Synthetic Lubrication*, 24:77–90.
- Therriault, D., Shepherd, R.F., White, S.R. and Lewis, J.A. 2005. "Fugitive Inks for Direct-write Assembly of Three-dimensional Microvascular Networks," *Advanced Materials*, 17:395–399.
- Therriault, D., White, S.R. and Lewis, J.A. 2003. "Chaotic Mixing in Three-dimensional Microvascular Networks Fabricated by Direct-write Assembly," *Nature Materials*, 2:265–271.
- Toohey, K.S., Sottos, N.R., Lewis, J.A., Moore, J.S. and White, S.R. 2007. "Self-healing Materials with Microvascular Networks," *Nature Materials*, 6:581–585.
- Tuckerman, D.B. and Pease, F.W. 1981. "High-Performance Heat Sinking for VLSI," *IEEE Electron Device Letters*, 2:126–129.
- Wang, Y., Yuan, G., Yoon, Y.-K., Allen, M.G. and Bidstrup, S.A. 2005. "Active Cooling Substrates for Thermal Management of Microelectronics," *IEEE Transactions on Components and Packaging Technologies*, 28:477–483.
- Wei, X.J., Joshi, Y. and Patterson, M.K. 2007. "Experimental and Numerical Study of a Stacked Microchannel Heat Sink for Liquid Cooling of Microelectronic Devices," *Journal of Heat Transfer-Transactions of the ASME*, 129:1432–1444.
- Yu, S. and Jung, D. 2008. "Thermal Management Strategy for a Proton Exchange Membrane Fuel Cell System with a Large Active Cell Area," *Renewable Energy*, 33:2540–2548.